the plant journal

SEB SOCIETY FOR EXPERIMENTAL BIOLOGY

The Plant Journal (2020) **102,** 703–717 doi: 10.1111/tpj.14655

PP7L is essential for MAIL1-mediated transposable element silencing and primary root growth

Cloe de Luxán-Hernández[1], Julia Lohmann[1], Wiebke Hellmeyer[1], Senoch Seanpong[1], Kerstin Wöltje[1], Zoltan Magyar[2], Aladár Pettkó-Szandtner[2,3], Thierry Pélissier[4], Geert De Jaeger[5,6], Stefan Hoth[1], Olivier Mathieu[4] and Magdalena Weingartner[1,*]

[1]*Molecular Plant Physiology, Institute for Plant Science and Microbiology, Universität Hamburg, Hamburg 22609, Germany,*
[2]*Institute of Plant Biology, Biological Research Centre, Szeged 6726, Hungary,*
[3]*Laboratory of Proteomics Research, Biological Research Centre, Temesvári krt. 62, 6726 Szeged, Hungary,*
[4]*GReD – CNRS UMR6293 – Inserm U1103, Université Clermont Auvergne, UFR de Médecine, Clermont-Ferrand Cedex, France,*
[5]*VIB Center for Plant Systems Biology, 9052 Gent, Belgium, and*
[6]*Department of Plant Biotechnology and Bioinformatics, Ghent University, Technologiepark 71, 9052 Gent, Belgium*

Received 21 March 2019; revised 22 November 2019; accepted 4 December 2019; published online 17 December 2019.
*For correspondence (e-mail magdalena.weingartner@uni-hamburg.de).

SUMMARY

The two paralogous Arabidopsis genes *MAINTENANCE OF MERISTEMS (MAIN)* and *MAINTENANCE OF MERISTEMS LIKE1 (MAIL1)* encode a conserved retrotransposon-related plant mobile domain and are known to be required for silencing of transposable elements (TE) and for primary root development. Loss of function of either *MAIN* or *MAIL1* leads to release of heterochromatic TEs, reduced condensation of pericentromeric heterochromatin, cell death of meristem cells and growth arrest of the primary root soon after germination. Here, we show that they act in one protein complex that also contains the inactive isoform of PROTEIN PHOSPHATASE 7 (PP7), which is named PROTEIN PHOSPHATASE 7-LIKE (PP7L). PP7L was previously shown to be important for chloroplast biogenesis and efficient chloroplast protein synthesis. We show that loss of *PP7L* function leads to the same root growth phenotype as loss of *MAIL1* or *MAIN*. In addition, *pp7l* mutants show similar silencing defects. Double mutant analyses confirmed that the three proteins act in the same molecular pathway. The primary root growth arrest, which is associated with cell death of stem cells and their daughter cells, is a consequence of genome instability. Our data demonstrate so far unrecognized functions of an inactive phosphatase isoform in a protein complex that is essential for silencing of heterochromatic elements and for maintenance of genome stability in dividing cells.

Keywords: *Arabidopsis thaliana*, meristems, root growth architecture, DNA repair and processing, transcriptional regulation.

INTRODUCTION

Almost all cells of the plant body descend from small populations of self-renewing stem cells that are maintained within meristems. The stem cell niche of the root apical meristem (RAM) is located at the growing tip of the root and consists of a small group of rarely dividing quiescent centre (QC) cells, which are believed to act as organizers and as long-term reservoirs of stem cells (Heidstra and Sabatini, 2014). The cells directly adjacent to the QC are named root initials and maintain a stem cell-like character. They are able to renew themselves and to produce daughter cells, which undergo several rounds of rapid cell divisions until reaching the elongation zone, in which they gradually become differentiated (Wendrich *et al.*, 2017a). During cell division, the status and integrity of the DNA is constantly monitored and detection of DNA damage leads to activation of the two conserved checkpoint kinases ATAXIATELANGIECTASIA MUTATED (ATM) and ATM AND RAD3-RELATED (ATR), which are known to phosphorylate the transcription factor SUPPRESSOR OF GAMMA-RESPONSE 1 (SOG1) in plants (Sancar *et al.*, 2004; Yoshiyama *et al.*, 2013). Once being activated, SOG1 orchestrates the DNA damage response (DDR) involving delayed cell cycle progression by transcriptional induction of cell cycle inhibitors and activation of DNA repair by induction of DNA repair factors (Culligan *et al.*, 2006; Yoshiyama *et al.*, 2009; Yi *et al.*, 2014). In addition, SOG1 induces programmed cell death (PCD) specifically in root initials to prevent accumulation and propagation of

deleterious mutations (Furukawa *et al.*, 2010; Johnson *et al.*, 2018). New pools of stem cells are then replenished by activation of cell division in QC cells, which allows the formation of a new stem cell niche that sustains root growth (Heyman *et al.*, 2013; Hu *et al.*, 2016). Therefore, treatment of Arabidopsis seedlings with DNA damaging agents such as zeocin or bleomycin or with ionizing radiation leads to activation of DDR, resulting in a transient arrest of root growth and induction of cell death specifically in root initials and their immediate descendants (Fulcher and Sablowski, 2009; Furukawa *et al.*, 2010). In agreement, impaired root growth and spontaneous cell death in the RAM was also described for mutants with defects in DNA replication, DNA repair, or chromatin assembly. Examples are mutants lacking components of the mediator complex (Raya-Gonzalez *et al.*, 2018) or with disrupted function of the homologue of yeast *DNA Replication Helicase/Nuclease 2* (Jia *et al.*, 2016), as well as mutants with impaired function of histone chaperone complexes (Ma *et al.*, 2018) or with defects in structural components of the chromatin (Diaz *et al.*, 2019).

We have previously characterized the *MAINTENANCE OF MERISTEMS* (*MAIN*) gene family, which is defined by a conserved amino-transferase-like plant mobile domain (PMD) of unknown function (Uhlken *et al.*, 2014a). Two members of this gene family, namely *MAIN* and *MAIN-LIKE 1* (*MAIL1*) are important for maintenance of genome stability in dividing cells of the RAM. Our published data showed that the single loss-of-function *main-2* and *mail1-1* mutants displayed very strong developmental defects, in particular a short-root phenotype due to growth arrest of the primary root soon after germination. This phenotype was associated with reduced cell division and precocious differentiation in the RAM, death of stem cells and their progenitor cells, and progressive loss of QC identity (Wenig *et al.*, 2013; Uhlken *et al.*, 2014b). Moreover, genome-wide expression analyses revealed that several TE-encoded loci that were mainly localized in pericentromeric heterochromatin were overexpressed in both mutants. Constitutive heterochromatin is in all eukaryotes highly condensed, transcriptionally inactive and enriched with different kinds of repeated sequences and TEs, while the gene-rich euchromatin is more relaxed and transcriptionally active (Fransz and de Jong, 2002). Condensation of heterochromatin is, in most plant cells, mediated by high levels of cytosine methylation and repressive histone modifications (Du *et al.*, 2015). In addition, silencing is ensured by factors that control proper chromatin condensation and thus act independently of DNA methylation (Moissiard *et al.*, 2012; Feng and Michaels, 2015; Wang *et al.*, 2017). The overexpressed loci in *main* and *mail1-1* exhibited no changes in the pattern of DNA methylation and histone modification (Uhlken *et al.*, 2014a,b; Ikeda *et al.*, 2017). This suggested that they may be involved in heterochromatin silencing by influencing chromatin structure and function (Ikeda *et al.*, 2017).

Apart from *MAIN* and *MAIL1*, the *MAIN* gene family contains two additional members named *MAIN-LIKE2* (*MAIL2*) and *MAIN-LIKE3* (*MAIL3*). Whereas *MAIN, MAIL1*, and *MAIL2* encode very similar proteins, *MAIL3* encodes a larger protein that contains an additional phosphatase domain. For that reason, MAIL3 also groups with the plant-specific PP7-type family of serine/threonine phosphatases (Uhrig *et al.*, 2013). In Arabidopsis, the PP7-type subfamily has three members: the founding member PROTEIN PHOSPHATASE 7 (PP7), MAIN-LIKE 3 (MAIL3), and an inactive isoform encoded by the At5g10900 locus, which is named PP7L (Uhrig *et al.*, 2013) (Xu *et al.*, 2019). The function of MAIL3 is unknown and T-DNA insertion lines for *MAIL3* are indistinguishable from wild-type (Uhlken *et al.*, 2014b). PP7 was identified as an important modulator of light signalling by influencing the expression of nuclear-encoded sigma factors (SIG), which are important regulators of chloroplast gene expression (Moller *et al.*, 2003; Genoud *et al.*, 2008; Sun *et al.*, 2012). Recently, T-DNA insertion mutants for *PP7L* have been shown to exhibit impaired chloroplast development specifically during young seedling development. This was associated with impaired chloroplast ribosome accumulation and reduced protein synthesis in chloroplasts. However, the mechanism by which PP7L influences chloroplast translation is still unknown (Xu *et al.*, 2019). Here, we aimed at understanding the molecular mechanisms of MAIN and MAIL1 action. We show that MAIN and MAIL1 interact with each other and with PP7L. Loss-of-function alleles for *PP7L* displayed the same developmental defects as mail1-*1* and *main-2* mutants, including growth arrest of the primary root and cell death in the RAM. Moreover, *PP7L* mutant lines showed mis-expression of a subset of heterochromatic TE-encoded loci, which are also mis-expressed in *mail1-1* and *main-2*. Double mutant analyses confirmed that MAIN, MAIL1 and MIPP acted in the same pathway and suggest that MAIL3 might influence the silencing activity of this complex. In addition, we show evidence that the primary root growth defects in these mutants were caused by genome instability.

RESULTS

MAIL1 interacts with MAIN and PP7L

To gain insight into molecular functions of MAIN family proteins, we searched for proteins interacting with MAIL1. To this aim, co-immunoprecipitation (Co-IP) experiments were performed using *mail1-1* mutant seedlings expressing a *MAIL1–green fluorescent protein (GFP)* fusion from the endogenous *MAIL1* promoter (*mail1-1/pMAIL1::MAIL1–GFP*), which fully complemented the

mutant phenotype (Uhlken *et al.*, 2014b). MAIL1–GFP and putative interaction partners were identified by immunoprecipitation followed by tandem mass spectrometry (IP-MS/MS). In parallel, two control Co-IP experiments using a line expressing GFP (*p35S::GFP*) were performed. MAIN and PROTEIN PHOSPHATASE 7-LIKE (PP7-L), which is encoded by the At5g10900 gene, were among the proteins that specifically and most abundantly co-purified with MAIL1–GFP in each of the three experiments (Table S1). We performed reverse Co-IP experiments to confirm these co-purifications using seedlings expressing PP7L–GFP from its native promoter as bait. Indeed, peptides for MAIN and MAIL1 were most abundantly identified in the co-immunoprecipitates of PP7-L–GFP in the three independent experiments (Table S1). Therefore, MAIN, MAIL1, and PP7L belong to the same protein complex in plant cells. Yeast-two-hybrid (Y2H) experiments were performed to further address the physical interaction of MAIL1 with MAIN and of MAIL1 with PP7L. A full-length construct of MAIL1 showed strong interaction with PP7L and weaker interaction with MAIN (Figure 1a). In contrast, a truncated version of MAIL1, in which the non-conserved C-terminal domain was deleted (MAIL1ΔC), did not interact with PP7L showing that the conserved PMD domain of MAIL1 was not sufficient for this interaction (Figure 1a,b). To confirm the observed interactions *in planta*, we performed bimolecular fluorescence complementation (BiFC) experiments using the pBiFCt-2in1 vector system in Arabidopsis leaf protoplasts (Grefen and Blatt, 2012). Constructs harbouring full-length open reading frames of *MAIL1* and *MAIN*, *MAIL1* and *PP7L*, or *MAIN* and *PP7L*, which were fused at the N-terminus to each half of the *yellow fluorescent protein (YFP) resulted in* a bright YFP-derived fluorescence signal, which was mainly seen in the nucleus (Figure 1c). No fluorescence was detected in control experiments, in which PP7L fused to the C-terminal half of YFP and no protein fused to the N-terminal half of YFP was expressed (Figure 1c). We have previously shown that GFP fusion proteins of MAIL1 or MAIN were exclusively localized to the nucleus (Wenig *et al.*, 2013; Uhlken *et al.*, 2014a,b). In contrast, the PP7L–GFP fusion protein was reported to be localized to the nucleus and to the cytoplasm (Xu *et al.*, 2019). We therefore analyzed the co-localization of PP7L–GFP and MAIL1–mCherry in tobacco leaf epidermis cells, in which both constructs were simultaneously expressed from estradiol-inducible promoters. We found that the MAIL1–GFP signal was confined to the nucleus while PP7L–mCherry derived fluorescence accumulated in both the nucleus and the cytoplasm (Figure 1d). Taken together, these results showed that MAIL1 physically interacted with MAIN and with PP7L, and that this complex localized to the nucleus, while PP7L by itself accumulated also in the cytoplasm.

Loss-of-function mutants for PP7L phenocopy *mail1-1* mutants

To test the biological significance of the interaction between MAIL1 and PP7L, we obtained T-DNA insertion lines for *PP7L* from the SALK collection (Alonso *et al.*, 2003), which were previously characterized and named *pp7l-1* and *pp7l-3* (Xu *et al.*, 2019). Our phenotypic analysis of seedlings revealed that homozygous *pp7l-1* and *pp7l-3* mutants displayed the similar primary root growth defect as the *mail1-1* and *main-2* mutant (Figure 2a). By measuring root length of seedlings growing for 15 days on vertical agar plates, we found that growth arrest of the primary root occurred in *mail1-1, pp7l-1* and *pp7l-3* at 3 days after germination (dag), while in *main-2* the primary root continued to grow, although much slower than the wild-type primary root (Figure 2b). Confocal microscopy of propidium iodide (PI)-stained root tips of seedlings at 3 dag revealed that the impaired growth of the primary root was associated with a reduced size of the cell division zone and early onset of cell differentiation (Figure 2c). Furthermore, PI staining that specifically marks dead cells due to impaired membrane integrity demonstrated that each of these mutant lines exhibited cell death of stem cells and their descendants. At 3 dag, seedlings of *mail1-1, pp7l-1* and *pp7l-3* were indistinguishable from each other and displayed numerous dead cells in the cell division zone and a disorganized cellular pattern of the RAM. In contrast, in the *main-2* mutant, the cellular organization of the RAM was maintained and only in about 50% of the seedlings ($n = 40$) individual dead cells were observed (Figure 2c). It was previously shown that embryo development was unaltered in the *mail1-1* mutant and that the defects in the RAM occurred only after onset of germination (Uhlken *et al.*, 2014b). We therefore examined embryo development of *pp7l-1* and *pp7l-3* mutants and found no difference from wild-type at any stage of development (Figure S1a,b). Moreover, the cellular pattern of the RAM was indistinguishable from wild-type in mature seeds of both *pp7l-1 and pp7l-3* mutant lines (Figure S1c). In a next step, we analyzed root tips of germinating seeds and found that during the process of radicle emergence (growth stage 0.50; Boyes *et al.*, 2001) numerous dead cells accumulated in the cell division zone of the RAM in the *pp7l-1*, *pp7l-3*, and *mail1-1* mutants. In contrast, in the *main-2* mutant most of the germinating seeds examined resembled wild-type and only in 12% of all roots ($n = 35$) dead cells were detected (Figure 2d). These analyses demonstrated that *pp7l-1* and *pp7l-3* showed the identical root growth defects as *mail1-1* whereas, in *main-2*, the same defects also occurred, but at a later developmental stage. Despite the growth arrest of the primary root, *pp7l-1* and *pp7l-3* mutant lines were able to sustain shoot growth by forming anchor roots, which seemed to take over the function of

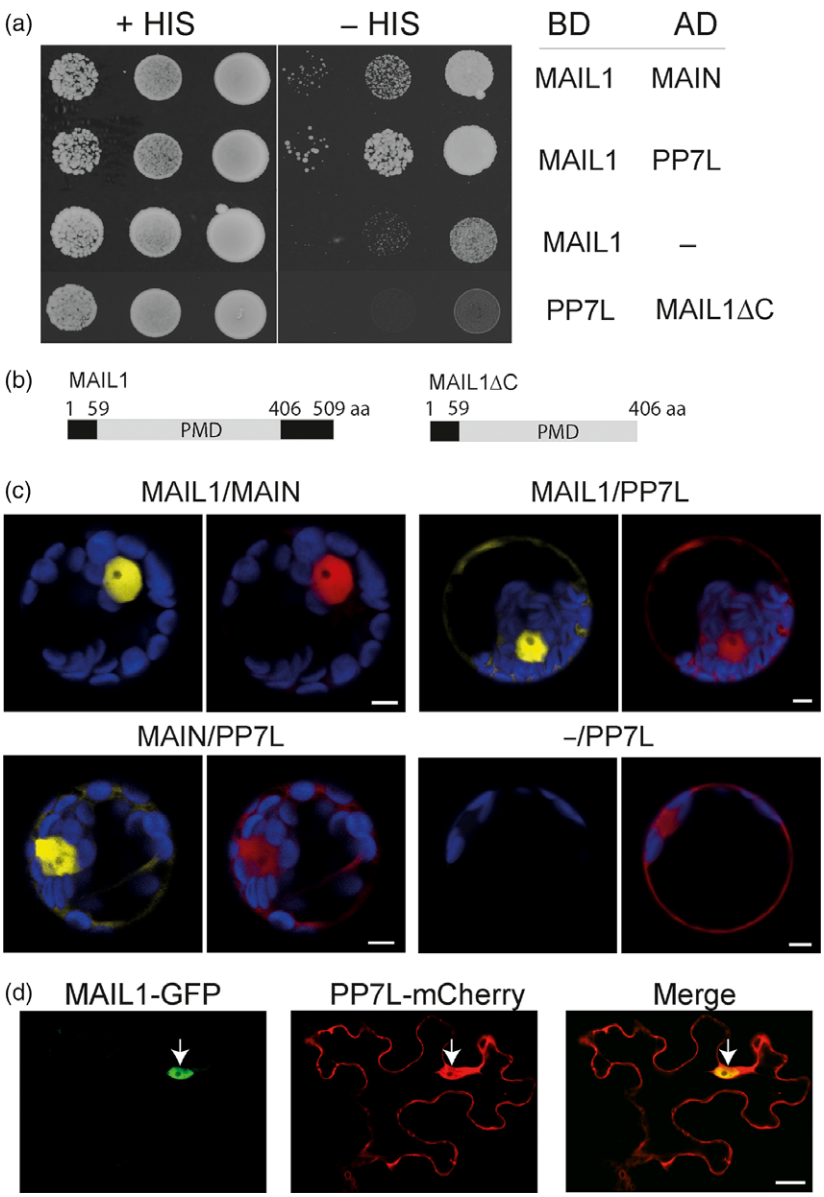

Figure 1. MAIL1 interacts with PP7L and with MAIN. (a) Yeast-two-hybrid (Y2H) assay showing the interaction of MAIL1 with PP7L and with MAIN. Growth of serial dilutions of yeast colonies was verified on medium without tryptophan and leucine (+HIS) and selective medium without tryptophan, leucine and histidine (–HIS) supplemented with 3-amino-1,2,4-triazole (3-AT). BD, DNA-binding domain; AD, activation domain. An empty AD-containing vector was used as the control.
(b) Structure of the MAIL1 full-length protein and the truncated version of MAIL1 (MAIl1ΔC) with the plant mobile domain (PMD) highlighted in grey.
(c) BiFC assays showing that Arabidopsis leaf protoplasts transfected with pBiFCt-2in1-NN (MAIL1/MAIN), pBiFCt-2in1-NN (MAIL1/PP7L) or pBiFCt-2in1-NN (MAIN/PP7L) showed a yellow fluorescent protein (YFP)-derived fluorescence signal in the nucleus (arrows). Protoplasts transfected with a control construct (pBiFCt-2in1-NN (–/PP7L)) showed no YFP-derived fluorescence. Red: red fluorescent protein (RFP)-derived fluorescence as a control for successful transfection. Blue: autofluorescence of chloroplasts. Yellow: YFP-derived fluorescence. Scale bars, 5 μm.
(d) Representative confocal images of *Nicotiana benthamiana* epidermis cells co-expressing MAIL1–green fluorescent protein (GFP) and PP7L–mCherry showing that MAIL1–GFP-derived fluorescence (green) is confined to the nucleus and PP7L–mCherry-derived fluorescence (red) is seen in the nucleus and in the cytoplasm. Arrows point to the nucleus. Scale bar, 25 μm.

the primary root, as previously described for *mail1-1* (Uhlken *et al.*, 2014b). Both *pp7l* mutant lines formed rosettes of smaller size than wild-type and were delayed in development (Figure S2a) (Xu *et al.*, 2019). They produced the same number of rosette leaves before onset of flowering as wild-type, and during shoot and flower formation no phenotypic alterations were detected (Figure S2b,c). We assessed the tissue-specific *PP7L* expression pattern in wild-type plants and found that *PP7L* was ubiquitously expressed in all tissues tested including roots (Figure S2d). In conclusion, these analyses showed that PP7L was, like MAIN and MAIL1, essential for primary root growth during post-germination development in addition to its previously established function during chloroplast development in leaves (Xu *et al.*, 2019).

PP7L is involved in silencing of TEs

Previously, RNA-sequencing (RNA-seq) analyses revealed that loss of *MAIL1* or *MAIN* induced release of silencing of numerous TEs belonging to both DNA transposon and retrotransposon classes. In addition, the expression of several protein-coding genes known to be epigenetically regulated was increased (Ikeda *et al.*, 2017). To test if PP7L was also involved in silencing of TEs, we selected six of those loci including two CACTA-like transposase family genes (*At1g36680* and *At5g33395*), the Mutator-like transposable element MULE gene *At2g15810*, the protein-coding gene *AT3g29639*, which was shown to be epigenetically regulated (Kurihara *et al.*, 2008), the DNA/HARBINGER transposon encoded gene *At4g04293* (*ATIS112A*) and the Gypsy

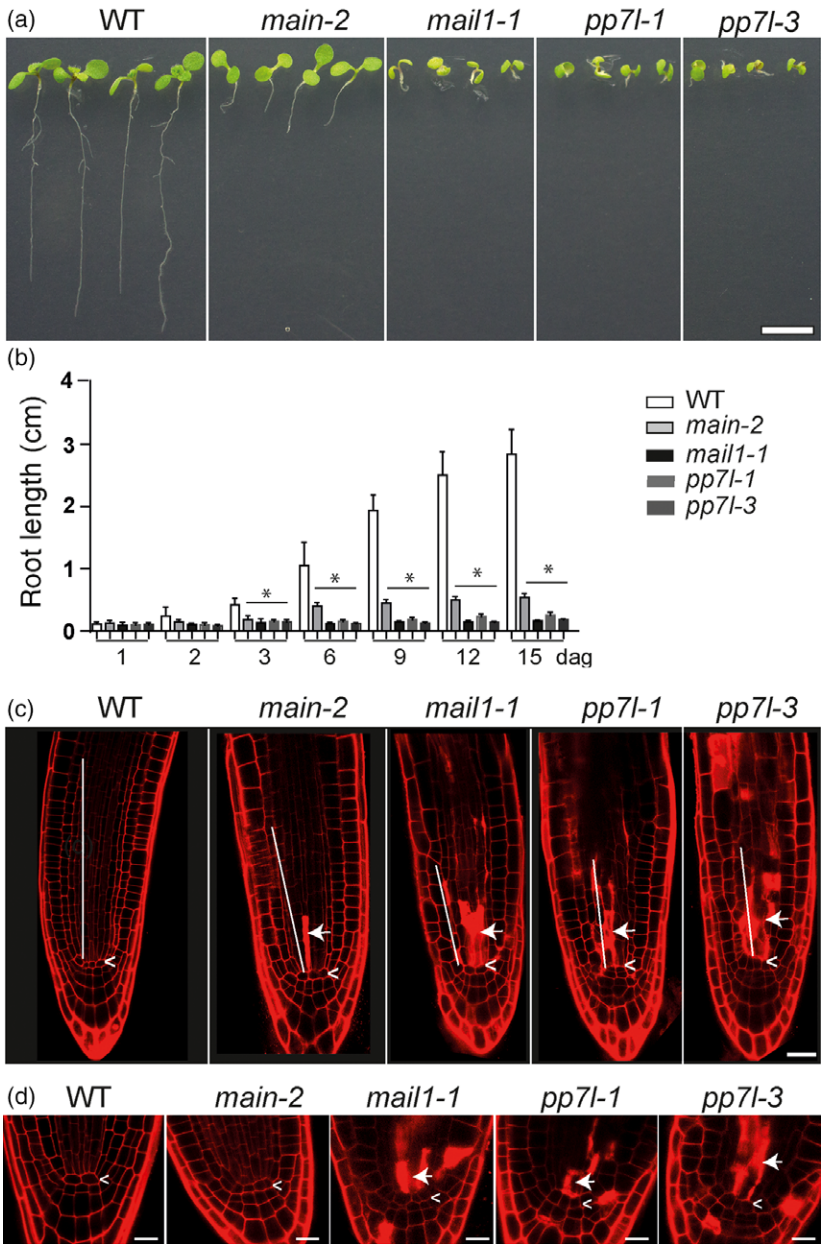

Figure 2. *pp7l-1* and *pp7l-3* showed similar developmental defects as *mail1-1 and main-2.*

(a) Representative images of wild-type, *main-2*, *mail1-1*, *pp7l-1*, and *pp7l-3* seedlings at 8 days after germination (dag). Scale bar, 0.7 cm.

(b) Wild-type and mutant seedlings were grown on vertical plates and root lengths were measured at indicated days after germination (dag). The mean of the root length of three independent experiments is shown. Graphs represent mean ± SE (n = 80–100). Asterisk indicate significant difference to wild-type ($P < 0.05$).

(c) Confocal images of propidium iodide (PI)-stained root tips of wild-type, *mail1-1, main-2, pp7l-1* and *pp7l-3* at 3 dag showing reduced size of the meristematic zone of the root apical meristem (RAM) (indicated by a white line) and accumulation of dead cells proximal to the quiescent centre (QC) in *mail1-1, main-2, pp7l-1, and pp7l-3* mutants. Arrows point to intensely stained, dead cells; arrowheads mark the position of the QC. Scale bar, 25 μm.

(d) Confocal images of PI-stained root tips of germinating seeds (24–48 h in light) of the indicated genotypes showing accumulation of dead cells around the QC (marked by arrowhead) in *mail1-1, pp7l-1 and pp7l-3* but not in wild-type or *main-2*. Arrows point to intensely stained, dead cells. Scale bars, 12.5 μm.

LTR-retrotransposon encoded locus *ATHILA* (*At3TE58495*). In the following, we tested by RT-qPCR whether these loci were also mis-expressed in *pp7l-1* and *pp7l-3*. Indeed, each of the six loci was significantly increased compared with wild-type in seedlings of *pp7l-1* and *pp7l-3* and they were expressed at similar levels when compared with *mail1-1* and *main-2* (Figure 3a). To ensure that the release of silencing was due to loss of *PP7L* function we analyzed the expression of these loci in a complementation line for *pp7l-1* (*pp7l-1*C). In this line, a construct carrying the genomic sequence of *PP7L* fused at the C-terminus to GFP was expressed under its native promoter on the *pp7l-1* mutant background. In *pp7l-1C*, the expression of each of the tested loci was reduced to wild-type levels (Figure 3a). We also confirmed that the primary root was fully restored in seedlings of *pp7l-1-C* grown on Murashige and Skoog plates (Figure 3b). Confocal imaging of root tips revealed that there was no cell death in the division zone of the RAM of *pp7l-1C* seedlings and a PP7L–GFP-derived signal was observed in all cells of the root tip (Figure 3c). To further confirm that PP7L was involved in TE silencing, we analyzed the recently published RNA-seq dataset for *pp7l-1* (Xu *et al.*, 2019) for TE expression and found that 11 TE-encoded loci were among the significantly increased transcripts. Notably, 10 of these loci were among the transcripts that were also found as upregulated in the

published RNA-seq datasets for *mail1-1* and *main-2* (Ikeda *et al.*, 2017) (Figure 3d and Table S2). It should be noted that two of the loci that showed significant increase in both *pp7l-1* and *pp7l-3* in our RT-qPCR experiments, namely At1g6680 and At3TE58495, were not detected as significantly upregulated in the *pp7i-1* RNA-seq data. This difference might be explained by the different growth conditions or age of the sampled seedlings: for the *pp7-1* RNA-seq analysis 4-day-old seedlings were used, whereas we used samples of 6-day-old seedlings. Taken together, these data demonstrated that loss of *PP7L* function caused not only the same root growth phenotype as loss of *MAIL1* or *MAIN*, but that PP7L was also important for the silencing of TE-encoded transcripts that were commonly controlled by MAIN and MAIL1.

MAIL1, MAIN, and PP7L function in the same molecular pathway

To confirm that PP7L acted in the same pathway as MAIL1 and MAIN, we generated *pp7l-1 mail1-1* and *pp7l-1 main-2* double mutants. We found that seedlings of both double mutant combinations showed growth arrest of the primary root and were phenotypically indistinguishable from the respective single mutant parents (Figure 4a). This indicated that MAIL1, MAIN, and PP7L function in the same pathway to support root growth. In a next step, we examined the expression levels of the six selected TE loci in both double mutant combinations and compared these to the respective single mutant parents (Figure 4b). We found no significant increase in the expression level of none of the tested loci in both double mutant lines compared with the single mutant parents, indicating that there was no additive effect on the strength of silencing release in the double mutant lines. However, we found that four loci were even significantly lower expressed in the *pp7l-1 main-2* double mutant compared with *pp7l-1*, and one of these was also reduced in the *pp7l-1 mail1-1* double mutant (Figure 4b). This might be explained by alternative silencing pathways, which try to compensate for loss of MAIN/MAIL1/PP7L activity and which might be more effective in the absence of two components of the complex. We have previously shown that the release of silencing in the *mail1-1* and *main-2* mutant was associated with impaired heterochromatin condensation (Ikeda *et al.*, 2017). By measuring chromocentre area in DAPI-stained nuclei we found a similar expansion of chromocentres in *pp7l-1* as we previously found for *mail1-1* (Ikeda *et al.*, 2017) and this was unchanged in the *pp7l-1 mail1-1* double mutant (Figure S3). Together, our results showed that the tested double mutant combinations had no general additive effect on silencing release and heterochromatin condensation, suggesting that PP7L, MAIL1, and MAIN acted in the same silencing pathway.

MAIL3 does not affect the root growth phenotype, but seems to influence PP7L-mediated TE silencing

The MAIL3 protein represents a long isoform of PP7. It contains a PMD domain sharing 34% identity with the PMD domain of MAIL1 and a PP7-like phosphatase domain sharing 39% identity with the phosphatase domain of PP7L (Figure 5a). In a complex with MAIL1 and/or MAIN proteins, PP7L may therefore form a protein similar to MAIL3. In contrast with MAIL3, however, PP7L is missing essential amino acids within its catalytic domain (Figure S4). Consequently, it is annotated as an inactive isoform (Farkas *et al.*, 2007). It has been shown that inactive phosphatase homologues can modulate or regulate signalling pathways of real phosphatases by acting as pseudophosphatases that bind to specific residues of their substrates and, in this way, protect these from becoming dephosphorylated by the real phosphatase (Reiterer *et al.*, 2014). We therefore wanted to test whether MAIL3 affects the function of the MAIN/MAIL1/PP7L complex. For instance, PP7L might act as a negative regulator of the MAIL3 phosphatase by binding to its (so far unknown) substrates and thereby preventing their de-phosphorylation. In this case, the *PP7L* mutant phenotype would be due to ectopic activity of MAIL3 and should be rescued in a *mail3-2* mutant background. We therefore generated double mutants between *pp7l-3* and *mail3-2 and* also between *mail1-1* and *mail3-2*. As shown previously, the *mail3-2* mutant has, like the pp7l-3 mutant, a T-DNA insertion within the phosphatase domain (Figure 5a). The *mail3-2* mutant did neither show any defect in development nor release of gene silencing (Uhlken *et al.*, 2014b; Ikeda *et al.*, 2017). We found that primary root growth arrest in the *pp7l-3 mail3-2* and in the *mail3-2 mail1-1* double mutant was indistinguishable from the arrest in *pp7l-3* or in *mail1-1*, indicating that the absence of MAIL3 did not influence the root growth defects (Figure 5b). In a next step, we tested whether the silencing activity of MAIL1 or PP7L was altered in the absence of MAIL3. RT-qPCR analyses revealed that each of the six tested loci was still significantly increased in expression in both double mutant combinations compared with wild-type or to the *mail3-2* single mutant (Figure 5c). However, whereas there was no significant difference in expression level of any of the tested loci between *mail1* and *mail3-2 mail1-1*, the expression level of four loci was significantly reduced in the *mail3-2 pp7l-3* double mutant compared with the *pp7l-3* single mutant (Figure 5c). This result indicated that MAIL3 does influence silencing activity of loci that are controlled by PP7L. Loss of *MAIL3* might either allow for more efficient residual silencing activity of MAIN and MAIL1 in the absence of PP7L or enable alternative silencing pathways to become more effective.

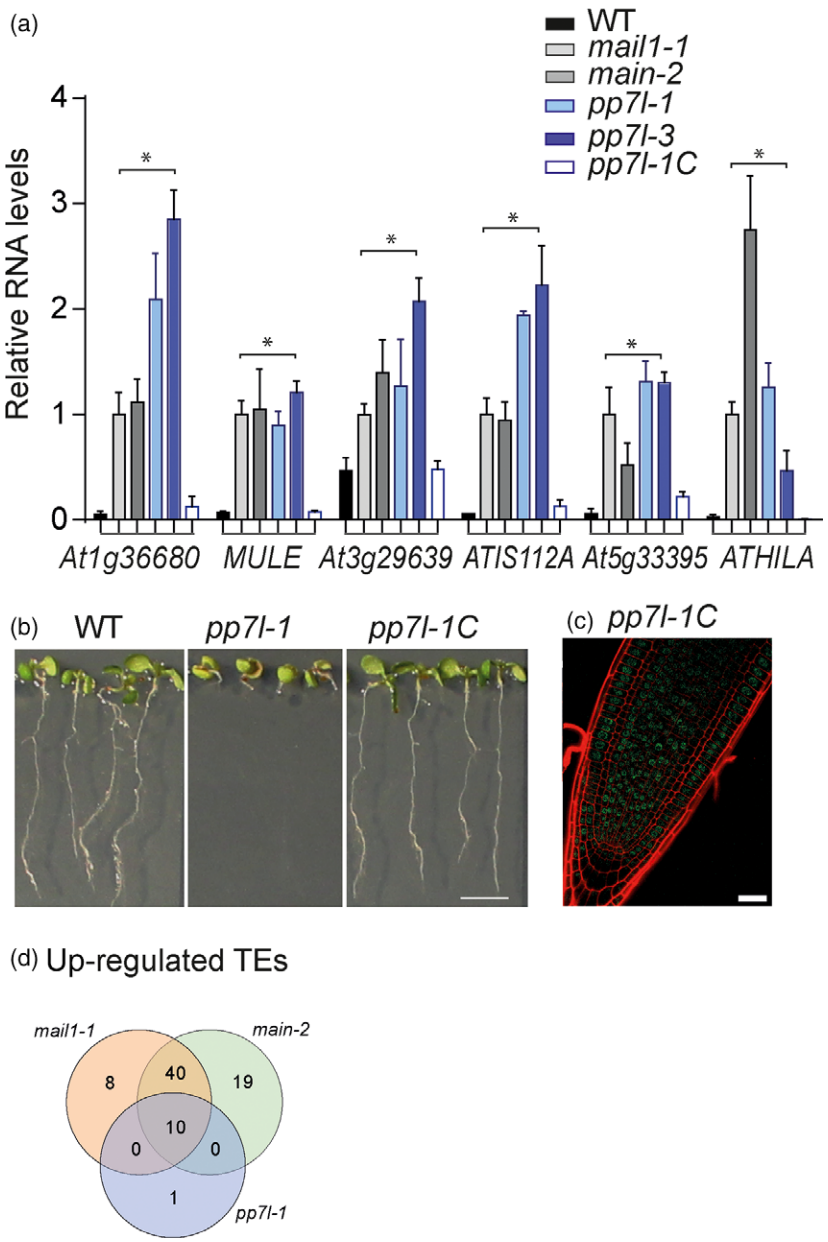

Figure 3. Loss of PP7L function lead to release of transposable element (TE) silencing.
(a) RT-qPCR analysis on RNA isolated from 7 days after germination (dag) seedlings of the indicated genotypes for six loci that were upregulated in mail1-1 and main-2. Transcript levels are represented relative to those in mail1-1, which were set to 1. Values represent the mean from three biological replicates ± SE. Asterisk indicates means differing significantly from wild-type ($P < 0.05$).
(b) Phenotype of 10-dag seedlings of wild-type (left), *pp7l-1* (centre) and *pp7l-1* mutants complemented with a ProPP7L:PP7L–green fluorescent protein (GFP) construct (*pp7l-1*C), in which the short-root phenotype was restored. Scale bar, 0.5 cm.
(c) Representative confocal image of a propidium iodide (PI)-stained root tip of, *pp7l-1*C at 7 dag showing that root apical meristem (RAM) organization was restored. A faint PP7L–GFP-derived signal (green) was seen in all cells of the root tip. Scale bar, 25 μm.
(d) Venn diagram showing overlap of TEs that were significantly increased in *mail1-1*, *main-2*, and *pp7l-1*.

The cell death in the RAM was caused by genome instability

Having established that MAIN, MAIL1, and PP7L acted in the same complex to prevent primary root growth arrest, accumulation of dead cells in the RAM, and release of TE silencing, we next aimed at understanding the mechanisms causing the observed mutant phenotypes. It is well established that activation of PCD in root initials is an important response to DNA damage (Hu *et al.*, 2016) and that spontaneous cell death in the RAM is a characteristic feature of mutants with impaired genome stability (Nisa *et al.*, 2019). If cell death in *pp7l-1* and *pp7l-3* mutants was due to impaired genome stability, we would expect that the expression of DDR-related genes would be increased. To test this, we performed RT-qPCR analyses on RNA isolated from root tips of *pp7l-1* and *pp7l-3* seedlings, in which cell death was detected. Indeed, out of the four genes tested, three showed significantly increased expression in both mutant lines compared with wild-type (Figure 6a). These are the DNA repair gene *POLY (ADP-RIBOSE)-POLYMERASE1* (*PARP1)*, the cell cycle inhibitor *SIAMESE-RELATED* (*SMR7*), and the *ETHYLEN RESPONSE FACTOR 115* (*ERF115*), a transcription factor that is known to become activated after DNA damage-induced cell death in meristematic cells. The DNA repair gene *RAD51* that is involved in homologous recombination-mediated DNA repair

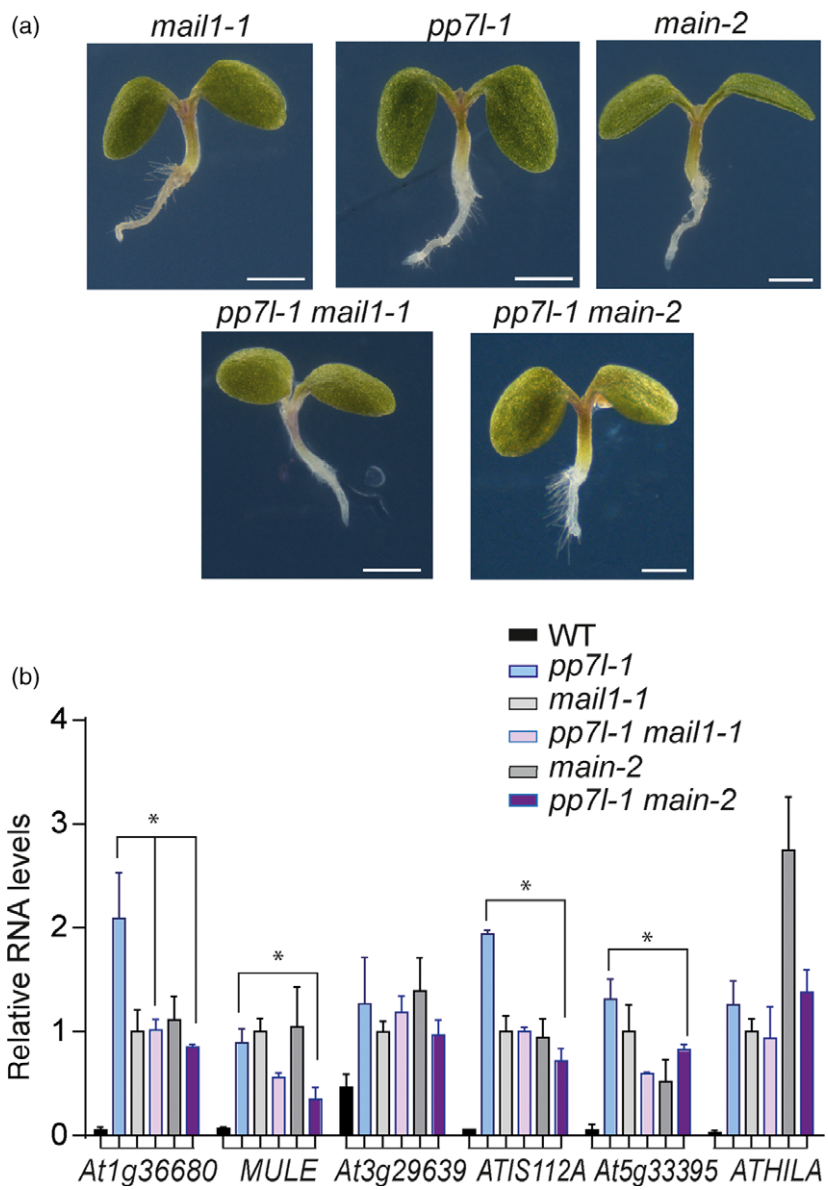

Figure 4. MAIL1, MAIN, and PP7L act in the same pathway.
(a) Representative photographs of 6 days after germination (dag) seedlings of the indicated genotypes showed that both double mutant combinations displayed the same phenotype as the single mutant parents. Scale bar, 1 mm.
(b) RT-qPCR analysis on RNA isolated from 7-dag seedlings of the indicated genotypes for the six selected loci showing that silencing strength was not increased in both double mutant combinations but at four loci reduced in *pp7l-1 main-2* compared with *pp7l-1*. Transcript levels are represented relative to those in *mail1-1*, which were set to 1. Values represent mean from three biological replicates ± SE. Asterisk indicates significant difference. ($P < 0.05$).

(Amiard *et al.*, 2013) was not increased in both mutant lines, indicating that this repair pathway might not be activated. A similar increased expression of DDR-related genes was previously shown to occur in root tips of *main-2* (Wenig *et al.*, 2013) and *mail1-1* (Uhlken *et al.*, 2014b) seedlings. The transcription factor SOG1 is an important regulator of DDR and is known to be required for induction of cell death in root initials upon DNA damage (Yoshiyama *et al.*, 2013). This cell-type-specific PCD is seen after a 20-h treatment with the radiometric drug zeocin in wild-type, but not in *SOG1*-deficient lines such as *sog1-1* (Yoshiyama *et al.*, 2013) or *sog1-7* (Figure S4) (Sjogren *et al.*, 2015). To test whether cell death in *ppl7* mutants was caused by constitutive activation of *SOG1* and thus could be rescued by inactivation of *SOG1*, we crossed the *pp7l-1* mutant onto the *sog1-7* mutant background. In PI-stained root tips of 3 dag seedlings we scored the fractions of roots showing either no cell death, cell death exclusively in one or two root initials or cell death in many cells of the RAM (Figure 6b,c). As expected, almost no cell death was observed in wild-type plants and in the *sog1-7* single mutants. In contrast, the *pp7l-1* mutant exhibited cell death in numerous cells across the mitotic zone of the RAM. This cell death pattern was almost unchanged in *pp7l-1 sog1-7* double mutants, indicating that cell death occurred independently of *SOG1*. In parallel, we analyzed a *main-2 sog1-7* double mutant. Whereas in the *main-2* single mutant the majority of seedlings showed no cell death or cell death confined to one or two root initials (Figure 6b,c), the *main-2 sog1-7* double mutant displayed in almost 100% of the roots death in

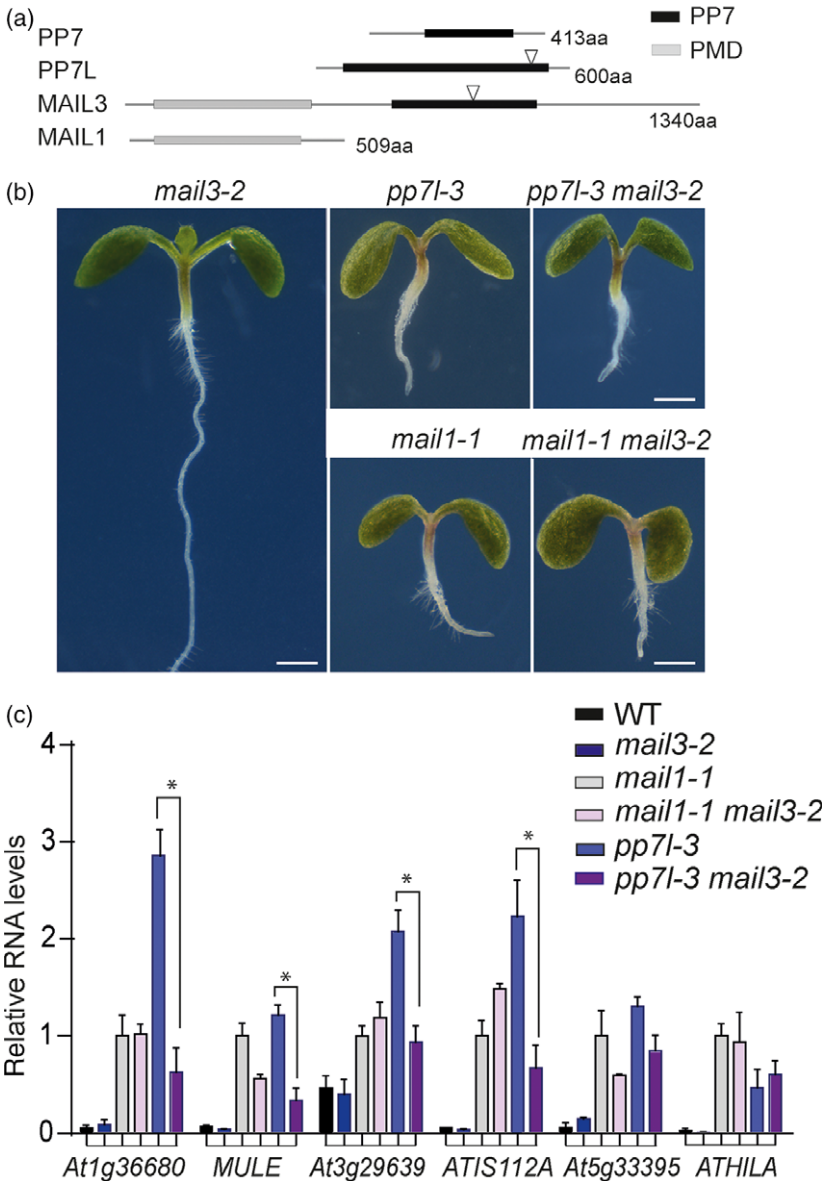

Figure 5. The phenotype of *pp7l-3* was unchanged on the *mail3-2* mutant background.
(a) Architecture of the PP7 (black) and PMD (grey) domain-containing proteins. Triangles indicate the position of the T-DNA insertion in *mail3-2* and *pp7l-3*.
(b) Representative photographs of 6 days after germination (dag) seedlings of the indicated genotypes showing that the short-root phenotype was unchanged in both double mutant combinations compared with the respective single mutants. Scale bar, 1 mm.
(c) RT-qPCR analysis on RNA isolated from 7-dag seedlings of the indicated genotypes for six heterochromatic loci showing that RNA levels were significantly reduced at four loci in the *pp7l-3 mail3-2* double mutant compared with *pp7l-3* while there was no significant difference between *mail1-1 mail3-2* and *mail1-1*. Transcript levels are represented relative to those in *mail1-1*, which were set to 1.
Values represent mean from three biological replicates ± SE. Asterisk indicates significant difference ($P < 0.05$).

many cells that were randomly distributed across the mitotic zone of the RAM (Figure 6b,c). The cell death pattern of the *main-2 sog1-7* double mutant was similar to that seen in *SOG-1* deficient lines after long-term exposure to genotoxic drugs (Figure S5). This *SOG-1* independent cell death was suggested to be a consequence of DNA repair processes not being efficiently activated and thus mitosis proceeding in the presence of damaged DNA (Furukawa *et al.*, 2010; Johnson *et al.*, 2018). This supported the conclusion that the cell death was caused by genome instability. In a next step, we tested whether *main-2* and *pp7l-1* were both able to transcriptionally respond to DNA damage treatment. To this end, seedlings of wild-type, *main-2* and *pp7l-1* were incubated for 2 h with the DNA damaging drug zeocin and used for RT-qPCR analysis of four well established DDR genes: *RAD51*, *BREAST CANCER SUSCEPTIBILITY1* (*BRCA1*), *POLY (ADP-RIBOSE)-POLYMERASE2* (*PARP2*) and *SIAMESE-RELATED 7* (*SMR7*). Both mutant lines showed a robust induction of each of these genes upon zeocin treatment, indicating that DDR signalling was not impaired (Figure 6d). Taken together, these results showed that loss of function of the MAIN/MAIL1/PP7L complex was associated with genome instability and consequent cell death in dividing cells. This cell death occurred through a pathway that acts independent of SOG1 signalling.

DISCUSSION

MAIN, MAIL1, and PP7L act in one protein complex

MAIL1 and MAIN belong to a small protein family that is characterized by the PMD domain, a conserved protein motif that is also found in several different transposon

encoded genes. The molecular function of this domain is still unknown. Single loss-of-function mutations for *MAIN* and *MAIL1* caused similar phenotypes (Wenig *et al.*, 2013; Uhlken *et al.*, 2014a,b), and these phenotypes were not changed in *main-2 mail1-1* double mutants. It was therefore suggested that the two proteins may act as a heterodimer (Ikeda *et al.*, 2017). Here, we showed that MAIN and MAIL1 indeed act in the same protein complex and that PP7L is part of this complex (Figure 1). Each of these three proteins contains a predicted nuclear localization signal (Kosugi *et al.*, 2009). Interestingly, we found that PP7L localized to the nucleus and to the cytoplasm, whereas MAIN and MAIL1 were exclusively localized to the nucleus (Figure 1), suggesting that interaction between the three proteins does only occur in the nucleus. It will be interesting to test how the intracellular localization of PP7L is regulated and whether its cytoplasmic accumulation serves a specific function.

PP7L is required for primary root development

PP7L belongs to the PP7-type family of serine–threonine phosphatases, which has a characteristic organization of its catalytic domain (Farkas *et al.*, 2007). PP7 is known as an important regulator of light signalling. A loss-of-function allele of PP7 displayed hypersensitivity to red light, and this phenotype was dependent on the presence of its interaction partner nucleotide-diphosphate kinase (NDPK2) (Genoud *et al.*, 2008). PP7 was also shown to positively regulate the blue light-induced stomatal opening by interacting and dephosphorylating the zinc-finger protein HYPERSENSITIVE TO RED AND BLUE1 (HRB1). Together PP7 and HRB1 seem to be part of a larger protein complex, which forms in a blue light-dependent manner (Sun *et al.*, 2012). Recently, three T-DNA insertion lines for *PP7L* (*pp7l-1*, *pp7l-2 pp7l-3*) were characterized and it was shown that PP7L is important for chloroplast biogenesis during development of cotyledons and the first pair of true leaves (Xu *et al.*, 2019). Each of these lines showed an increased accumulation of anthocyanins, a reduced photosynthetic activity, and delayed chloroplast development. This was associated with a reduced production of chloroplast proteins, and it was suggested that PP7L is involved post-transcriptional control of chloroplast gene expression (Xu *et al.*, 2019). In this study, we found that *pp7l-1* and*pp7l-3* mutants were also impaired in primary root development and showed growth arrest of the primary root, associated with cell death of dividing cells in the RAM. This cell death occurred in *pp7l-1* and *pp7l-3* during the process of germination (Figure 2) and thus even before the chloroplast development phenotype in cotyledons was observed (Xu *et al.*, 2019). We assume that the function of PP7L in chloroplast development is independent from its function in root development. However, further analyses are required to clarify this in future. The root growth phenotype of *pp7l* mutants was very similar to that of the single *mail1-1* or *main-2* mutants. We conclude that the presence of each of these three proteins is required for the function of the MAIL1/MAIN/PP7L protein complex in root development. Our double mutant analyses revealed no changes in the developmental phenotype in none of the combinations tested (*mail1-1 main-2*, *mail1-1 pp7l-1* and *main-2 pp7l-3)* (Figure 4), demonstrating that these three proteins function in the same molecular pathway. These analyses further confirmed that the observed phenotype is due to loss of MAIL1/MAIN/MIPP complex activity and not a consequence of ectopic accumulation of any of these three proteins in the absence of one interaction partner.

Potential role of PP7L in TE silencing

PP7L loss-of-function mutants did not only show the same root developmental defects as *mail1-1* and *main-2* but also release of the same TE-encoded loci. We show that only a subset of the loci that are commonly controlled by MAIN and MAIL1 was also mis-expressed in *pp7l-1*. One model to explain this could be that MAIL1 and MAIN act as a heterodimer to control silencing of heterochromatic loci. The association of PP7L to this heterodimer might be required for efficient silencing on a specific subset of the MAIN/MAIL1 controlled loci. It will be interesting to test in future experiments which domains are important for the interactions between these three proteins and how PP7L association influences the conformation of MAIN and MAIL1 proteins.

Due to mutations of essential amino acids within the serine/threonine-specific protein phosphatase signature, PP7L is annotated as catalytically inactive isoform, whereas MAIL3 and PP7 are both annotated as active phosphatases (Farkas *et al.*, 2007). It was tempting to speculate that a phosphatase-inactive MIPP acts as a negative regulator of MAIL3. Our double mutant analyses revealed that the root phenotype of *mail1-1* and *pp7l-3* was unaltered in the *mail3-2* mutant background (Figure 5b). However, the absence of MAIL3 did lead to a reduced expression level of several loci in the *pp7l-3* background (Figure 5c), whereas no changes were observed in the *mail1-1* background. One interpretation could be that MAIL3 influences the silencing efficiency of the MAIN/MAIL1 heterodimer only in the absence of PP7, for instance by destabilizing their interaction. Alternatively MAIL3 might influence the activity of alternative silencing pathways that try to compensate for the loss of MAIN/MAIL1/PP7L-mediated silencing.

How does the MAIL1/MAIN/PP7L complex control root growth and TE silencing?

We found that the first defect that was observed in the developing RAM of *mail1-1*, *main-2*, *pp7l-1*, and *pp7l-3* mutants was cell death of root initials and their descendants. This was especially obvious in the *main-2* mutant,

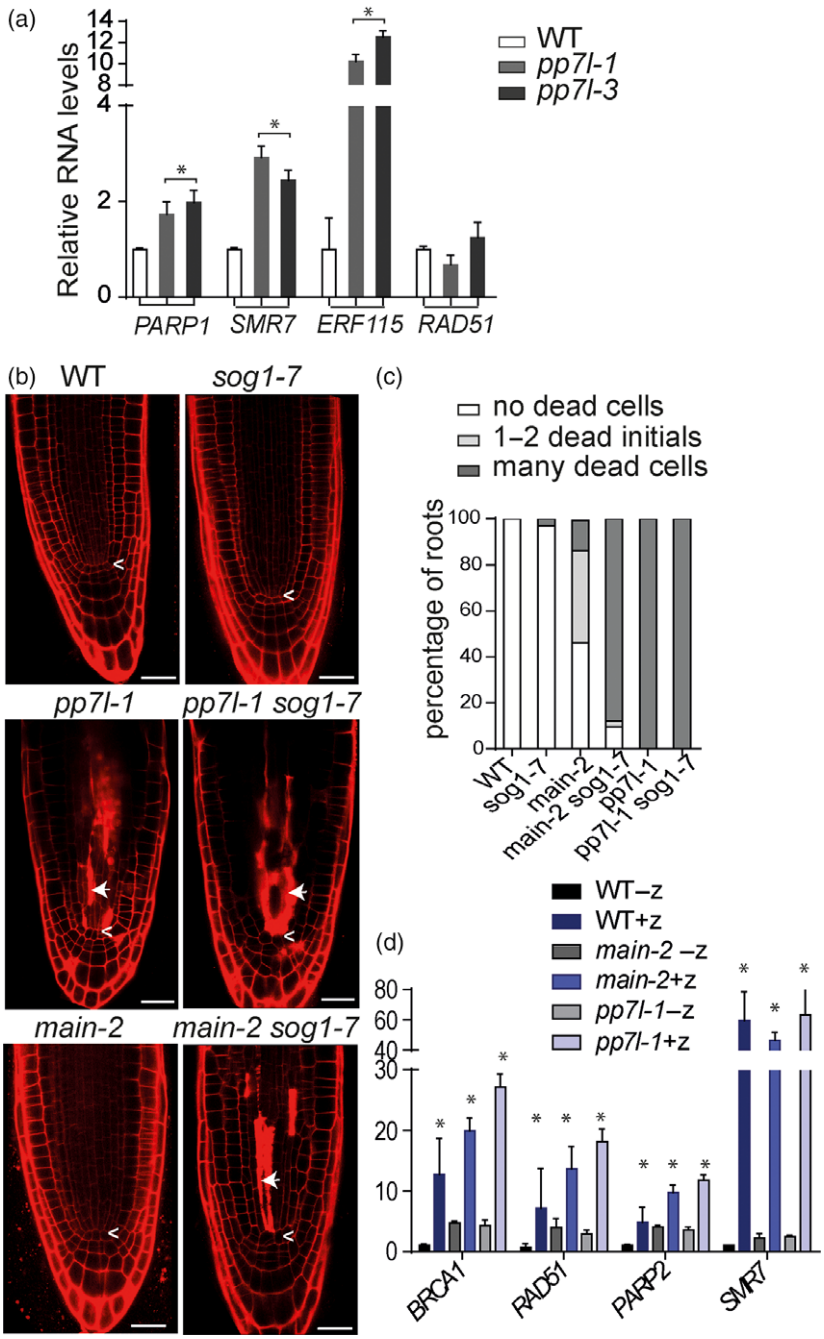

Figure 6. Analysis of DNA damage response (DDR) signalling and cell death in *pp7l* mutants.

(a) RT-qPCR analysis on RNA from root tips of 3 days after germination (dag) seedlings showed increased expression of DDR-related genes in *pp7l-1* and *pp7l-3*. Transcript levels are represented relative to those in wild-type, which were set to 1. Values represent mean from three biological replicates ± SE. Asterisk indicates significant difference from wild-type ($P < 0.05$).

(b) Representative confocal images of propidium iodide (PI)-stained root tips of 3 dag seedlings of the indicated genotypes. Arrows point to dead cells, arrowheads indicate the quiescent centre (QC). Scale bar, 25 μm.

(c) Quantification of roots of 3 dag seedlings showing no cell death, cell death in one or two root initials or cell death in many cells of the root apical meristem (RAM) of the indicated genotypes. Values represent mean from at least four biological replicates (n = 40–50).

(d) RT-qPCR analysis of DDR-related genes in 7-dag seedlings of the indicated genotypes with or without 2 h of zeocin (100 μM) treatment showed a robust transcriptional response to DNA damage in *main-2* and *pp7l-1*. Transcript levels are represented relative to those in wild-type without treatment, which were set to 1.

Values represent the mean from three biological replicates ± SE. Asterisk indicate means differing significantly from the respective control without zeocin treatment ($P < 0.05$).

in which the cell death phenotype occurred at a later stage than in *mail1*-1 and *pp7l* mutants (Figure 2). Moreover, published data showed that growth arrest of the primary root of *main-2* and *mail1-1* was associated with typical symptoms of active DDR such as reduced cell division, precocious cell differentiation in the RAM and increased expression of DNA repair genes (Wenig *et al.*, 2013; Uhlken *et al.*, 2014a,b). SOG1 is known to be activated upon DNA damage and on the one hand induces cell-type-specific PCD in root initials. On the other hand, SOG1 is essential for efficient activation of DNA repair pathways (Yoshiyama *et al.*, 2017). By analyzing *pp7l-1 sog1-7* and *main-2 sog1-7* double mutant lines (Figure 6), we established that cell death in the RAM was not induced by the SOG1 pathway. Moreover, the finding that the *main-2 sog1-7* double mutant showed more cell death than the *main-2* single mutant suggests that SOG1-mediated activation of DNA repair pathways is essential for cell survival during the first days after germination. We thus suggest that loss of function of *MAIN* and of its interaction partners *MAIL1* and

MIPP leads to genome instability and constitutive DNA damage resulting in root growth arrest. Recently, it was shown that in parallel to SOG1 another pathway involving the E2F transcription factors and RETINOBLASTOMA RELATED 1 (RBR1) controls the transcriptional response to DNA damage and the induction of cell death (Horvath *et al.*, 2017; Nisa *et al.*, 2019). It will be interesting to test whether this pathway is involved in the induction of cell death in the mutants described here. The next obvious question is how genome instability and the consequent defects in the RAM are connected with release of TE silencing. So far, release of TE silencing has not been associated with specific defects in the RAM. For instance loss of function of the chromatin remodelling factor DECREASED IN DNA METHYLATION (DDM1), which leads to high expression of numerous TEs due to loss of DNA methylation, is associated with accumulation of additional mutations in *ddm1-1* inbred lines (Tsukahara *et al.*, 2009). However, the *ddm1-1* mutant does not show any specific defects in root growth when grown under standard conditions (Choi *et al.*, 2019). One explanation could be that reduced compaction of pericentromeric heterochromatin, which was observed in *mail1-1*, *main-2*, and *pp7l-1* nuclei (Figure S3) and which was proposed to be responsible for release of silencing of pericentromeric heterochromatin (Ikeda *et al.*, 2017), might also lead to defects in chromatin integrity during cell divisions in the RAM. However, the fact that the severity of the root phenotype does not correlate with the release of silencing phenotype, for instance the pp7l-1 mutant lines show a stronger cell death phenotype but a weaker silencing defect compared with *main-2*, suggests that this is not the case. It seems more likely that the MAIN/MAIL1/PP7L complex functions in several different pathways and that the silencing defects occur independently from the meristem defects.

EXPERIMENTAL PROCEDURES

Plant material and growth conditions

Arabidopsis thaliana accession Columbia (Col) was used as the wild-type and all mutants are on the Col background. Plants were grown either in potting soil or on a solid medium containing half-strength Murashige and Skoog salts, 1% sucrose and 1% (w/v) agar in growth chambers (16 h light, 22°C/8 h dark, 18°C cycles). The T-DNA insertion lines SALK_018295 (mipp-1) and SALK_022053 were obtained through the Nottingham Arabidopsis Stock Centre. Primer pairs for genotyping are described in Table S2 (Alonso *et al.*, 2003). The T-DNA insertion lines for MAIN and MAIL1 and the sog1-7 mutant have been described previously (Wenig *et al.*, 2013; Uhlken *et al.*, 2014a,b; Sjogren *et al.*, 2015; Ikeda *et al.*, 2017).

Co-immunoprecipitation

Transgenic seedlings expressing MAIL1–GFP, MIPP–GFP or GFP were grown for 6 days and 3 g material was used for each GFP pull down. MS analysis was performed on a Q-Exactive Orbitrap and quantitative analysis was carried out using MaxQuant and Perseus software. Protocols are described in Wendrich *et al.* (2017b).

Plasmid construction

To create the complementation construct for *mipp-1* the genomic fragment of MIPP including the putative promoter sequence (310 bp upstream of Start-ATG) and excluding the STOP codon was amplified by PCR from genomic DNA and cloned into the pENTR-D-TOPO plasmid (www.thermofisher.com/) and sequenced. By LR recombination reaction, the fragment was inserted into the destination vector pMDC107 (Curtis and Grossniklaus, 2003) yielding ProPP7L-PP7L–GFP. For subcellular localization analysis, the full-length coding sequence (CDS) of MIPP and MAIL1 excluding the STOP codon was amplified by PCR and cloned into pDONR221, followed by LR recombination reaction with the destination vector pABindGFP (Bleckmann *et al.*, 2010). For Y2H assays, the full-length CDS of MAIN, MAIL1 and PP7L and the truncated version of MAIL1 (MAIL1ΔC) were amplified by PCR and cloned into pENTR-D-TOPO and the fragments were recombined into Gateway-compatible versions of the GAL4 DNA-binding domain vector pGBT-9 (Bleckmann *et al.*, 2010) and the activation domain vector pGAD424 (Clontech, www.takarabio.com) by LR recombination reaction. For BiFC analysis the full-length CDS of MAIN, MAIL1 and PP7L were amplified with primers adding recombination sites and cloned into pDONR221L1L4 or pDONR221L3L2 (Grefen and Blatt, 2012) and subsequently, by LR recombination reactions, inserted into BiFCt-2in1-NN. All primers are listed in Table S2.

Transgenic plants and transient expression in leaves

The constructs were transformed into *Agrobacterium tumefaciens* C58C1. To generate transgenic plants *Agrobacterium* was resuspended in 3 ml of transformation buffer containing 5% sucrose and 0.05% silwet L-77, and used for plant transformation by the floral dip method (Clough and Bent, 1998). For transient expression, the plasmid-containing agrobacteria were cultivated overnight at 28°C, harvested by centrifugation, and the pellet was resuspended in sterile water to a final OD_{600} of 1. The *Agrobacterium* suspension was infiltrated into leaves of 4- to 6-week-old *Nicotiana benthamiana* plants using a needleless 2-ml syringe.

Transformation of yeast cells

Transformation of the yeast strain AH109 was carried out according to (Gietz *et al.*, 1997). In brief, the binding and activation domain vectors were transformed simultaneously and the cells were spread on yeast minimal medium (SD medium: 0.66% yeast nitrogen base without amino acids, 0.066% amino acid mix, 2% glucose) lacking leucine and tryptophan (SD−L−W). After 3 d of incubation at 29°C, overnight cultures of single colonies were grown in double dropout medium (SD−L−W) under continuous shaking for 24 h at 29°C. The optical density was set to an OD_{600} of 4 and a dilution series from 10^{-1} to 10^{-3} was dripped on selection agar plates lacking histidine (SD−L−W−H) and containing 0.5 mM 3-amino-1,2,4-triazole (3-AT) as well as on SD−L−W medium as a control.

Protoplast isolation and transformation

Protoplast isolation was carried out as previously described with minor changes (Drechsel *et al.*, 2011). Mesophyll protoplasts were isolated from leaves of 6-week-old plants in protoplasting buffer (500 mM sorbitol, 1 mM $CaCl_2$, 0.25% macerozym R10, 1% cellulase R10, 10 mM MES-KOH, pH 5.7). The protoplast transformation was performed with 150 µl protoplasts, 20 µg plasmid DNA and 165 µl

PEG-Ca buffer (40% PEG 4000, 200 mM sorbitol, 100 mM $CaCl_2$). The transformation sample was mixed completely by gently rotating the tube and was incubated for 30 min at room temperature in the dark. To stop this process, the sample was diluted with W5 buffer (154 mM NaCl, 125 mM $CaCl_2$, 5 mM KCl, 5 mM glucose, 2 mM MES, pH 5.7) in three steps of 500 μl, 1 ml and 1.5 ml. The sample was centrifuged at 60 ***g*** for 3 min (without brake) and was washed with 3 ml W5 buffer twice. The protoplasts were incubated for 24 h at room temperature in the dark and fluorescence signals were analyzed by confocal laser scanning microscopy.

Root growth assay and propidium iodide staining

For the analysis of root growth, plants were germinated and grown on vertical plates. The plates were scanned every 3 days and measurement of root length was carried out using IMAGEJ software (http://imagej.nih.gov/ij/). The final values were calculated by determining the arithmetic mean of the root length values of three biological replicates, which were themselves the average of at least 20–30 plants. For treatment with zeocin, seedlings were transferred to liquid medium containing zeocin or, as control, no zeocin and incubated for the indicated time. Staining of cell wall and dead cells was performed by submerging seedling for 1 min in a 10 μg/ml PI/water solution and imaging was carried out using confocal microscopy.

Analysis of embryos and mature seeds

For analysis of embryonic development, seeds were excised from green siliques and cleared in Hoyer's solution (100 g chloral hydrate, 5 ml glycerol, 30 ml H_2O, 7.5 g gum arabic) overnight. Embryos were examined by confocal laser scanning microscopy using a differential interference contrast filter. For mPS-PI staining of mature seeds, dry seeds were incubated in water overnight and seeds with an opened seed coat were selected for further treatment. The seeds were treated as described in Truernit *et al.* (2008). In short, seeds were fixed (50% methanol, 10% acetic acid) at 4°C overnight, followed by an overnight treatment with 1% SDS and 0.2 N NaOH at RT. After bleaching using sodium hypochlorite solution (2.5% active chloride) for 5 min, seeds were treated with 1% periodic acid for 40 min at RT, and then stained with Schiff's reagent containing 100 μg/ml PI for 2 h. After two washing steps, seeds were destained in a chloral hydrate solution (4 g chloral hydrate, 1 ml glycerol, 2 ml water), covered with Hoyer's solution and incubated for 3 days before imaging by confocal microscopy.

Confocal laser scanning microscopy

To detect fluorescence of YFP, GFP or red fluorescent protein (RFP) confocal laser scanning microscopy was applied using the Leica TCS SP8 Confocal Platform (Leica Microsystems, Wetzlar, Germany). For excitation of YFP and GFP, laser light of 488 nm and for RFP of 561 nm was used. The detection windows ranged from 520 to 540 nm (YFP), 496–511 nm (GFP), 569–591 nm (RFP) and 690–708 nm for detection of chlorophyll auto-fluorescence.

Cytological analysis of nuclei

Determination of chromocentre area was performed on DAPI-stained nuclei from 4-week-old rosette leaves, as previously described (Ikeda *et al.*, 2017).

Expression analysis

Total RNA was extracted from Arabidopsis seedlings or inflorescence material using the innuPREP Plant RNA kit (Analytik Jena BioSolutions, www.analytik-jena.de). cDNA synthesis was performed using a QuantiTect® Reverse Transcription Kit (QIAGEN, http://www.qiagen.com). The cDNA was used either for semiquantitative PCR experiments or for quantitative PCR using a RotorGene 2000 (Corbett Research, http://www.corbettlifescience.com). Target-specific efficiencies were calculated as the mean of all reaction-specific efficiencies for a given target. Data were quality-controlled, normalized against two reference genes, and statistically evaluated using QBASEPLUS 3.0 (Hellemans *et al.*, 2007). Primers used for genotyping, semiquantitative reverse transcriptase polymerase chain reaction (RT-PCR) and qRT-PCR are listed in Table S3.

RNA-seq analysis

Previously published RNA-seq data of *pp7l-1* mutants (4-day-old seedlings, three replicates; (Xu *et al.*, 2019)), *mail1-1* and *main* mutants (3-week-old seedlings, two replicates; (Ikeda *et al.*, 2017)), and corresponding wild-types were mapped on the *Arabidopsis thaliana* genome (TAIR10) using STAR (Dobin *et al.*, 2013) allowing multimapping reads. Read counting was performed with featureCounts (Liao *et al.*, 2014) on 'transposable element' TAIR10 annotations. Differentially expressed TEs (Benjamini–Hochberg adjusted *P*-values < 0.05) were subsequently identified using DESEQ2 (Love *et al.*, 2014). TEs with $\geq$10% of the sequence overlapping a protein-coding gene annotation were not considered in the analysis.

ACCESSION NUMBERS

Sequence data from this article can be found in the EMBL/GenBank libraries under the accession numbers: *MAIL1* (At2g25010), *MAIL3* (At1g48120), *MAIN* (At1g17930), *PP7L* (At5g10900), *PP7* (At5g63870).

ACKNOWLEDGEMENTS

We thank Judith Mehrmann, Teresa Wulf, Sotoodeh Seyedehyasaman, and Zsuzsanna Darula for technical assistance and experimental support and to Paul Larsen (University of California, Riverside) for providing the seeds for the sog1-7 line. This work was funded by the Deutsche Forschungsgemeinschaft (DFG) grant to MW (WE 4506/6-1). C.L.-H. was supported by a UHH fellowship, work in the Mathieu lab was supported by CNRS, Inserm, and Université Clermont Auvergne and AP-Sz was supported by the GINOP-2.3.2-15-2016-00032.

CONFLICT OF INTEREST

The authors declare no conflicts of interest.

AUTHOR CONTRIBUTIONS

CL-H, JL, SS, and KW designed and performed experiments. WH and TP performed experiments. ZM and AP-S performed experiments and analyzed data. GJ, OM, and SH analyzed data. MW conceived this project, designed experiments, analyzed data and wrote the manuscript.

SUPPORTING INFORMATION

Additional Supporting Information may be found in the online version of this article.

Figure S1. Embryo development was unaffected in *pp7l-1* and *pp7l-3*.

Figure S2. Shoot development of *pp7l-1* and *pp7l-3*.

Figure S3. Impaired chromocentre condensation in *pp7l-1*.

Figure S4. PP7L is an inactive phosphatase.

Figure S5. Cell death pattern in the RAM of wild-type and *sog1-7* after zeocin treatment.

Table S1. Number of peptides identified by LC-MS/MS for co-immunoprecipitating proteins.

Table S2. Gene lists used to generate the diagram in Figure 3(d).

Table S3. Primer list.

REFERENCES

Alonso, J.M., Stepanova, A.N., Leisse, T.J. *et al.* (2003) Genome-wide insertional mutagenesis of *Arabidopsis thaliana*. *Science*, **301**, 653–657.

Amiard, S., Gallego, M.E. and White, C.I. (2013) Signaling of double strand breaks and deprotected telomeres in Arabidopsis. *Front. Plant Sci.* **4**, 405.

Bleckmann, A., Weidtkamp-Peters, S., Seidel, C.A. and Simon, R. (2010) Stem cell signaling in Arabidopsis requires CRN to localize CLV2 to the plasma membrane. *Plant Physiol.* **152**, 166–176.

Boyes, D.C., Zayed, A.M., Ascenzi, R., McCaskill, A.J., Hoffman, N.E., Davis, K.R. and Gorlach, J. (2001) Growth stage-based phenotypic analysis of Arabidopsis: a model for high throughput functional genomics in plants. *Plant Cell*, **13**, 1499–1510.

Choi, S.H., Ryu, T.H., Kim, J.I., Lee, S., Lee, S.S. and Kim, J.H. (2019) Mutation in DDM1 inhibits the homology directed repair of double strand breaks. *PLoS ONE One*, **14**, e0211878.

Clough, S.J. and Bent, A.F. (1998) Floral dip: a simplified method for Agrobacterium-mediated transformation of *Arabidopsis thaliana*. *Plant J.* **16**, 735–743.

Culligan, K.M., Robertson, C.E., Foreman, J., Doerner, P. and Britt, A.B. (2006) ATR and ATM play both distinct and additive roles in response to ionizing radiation. *Plant J.* **48**, 947–961.

Curtis, M.D. and Grossniklaus, U. (2003) A gateway cloning vector set for high-throughput functional analysis of genes in planta. *Plant Physiol.* **133**, 462–469.

Diaz, M., Pecinkova, P., Nowicka, A., Baroux, C., Sakamoto, T., Gandha, P.Y., Jerabkova, H., Matsunaga, S., Grossniklaus, U. and Pecinka, A. (2019) The SMC5/6 complex subunit NSE4A is involved in DNA damage repair and seed development. *Plant Cell*, **31**, 1579–1597.

Dobin, A., Davis, C.A., Schlesinger, F., Drenkow, J., Zaleski, C., Jha, S., Batut, P., Chaisson, M. and Gingeras, T.R. (2013) STAR: ultrafast universal RNA-seq aligner. *Bioinformatics*, **29**, 15–21.

Drechsel, G., Bergler, J., Wippel, K., Sauer, N., Vogelmann, K. and Hoth, S. (2011) C-terminal armadillo repeats are essential and sufficient for association of the plant U-box armadillo E3 ubiquitin ligase SAUL1 with the plasma membrane. *J. Exp. Bot.* **62**, 775–785.

Du, J., Johnson, L.M., Jacobsen, S.E. and Patel, D.J. (2015) DNA methylation pathways and their crosstalk with histone methylation. *Nat. Rev. Mol. Cell Biol.* **16**, 519–532.

Farkas, I., Dombradi, V., Miskei, M., Szabados, L. and Koncz, C. (2007) Arabidopsis PPP family of serine/threonine phosphatases. *Trends Plant Sci.* **12**, 169–176.

Feng, W. and Michaels, S.D. (2015) Accessing the inaccessible: the organization, transcription, replication, and repair of heterochromatin in plants. *Annu. Rev. Genet.* **49**, 439–459.

Fransz, P.F. and de Jong, J.H. (2002) Chromatin dynamics in plants. *Curr. Opin. Plant Biol.* **5**, 560–567.

Fulcher, N. and Sablowski, R. (2009) Hypersensitivity to DNA damage in plant stem cell niches. *Proc. Natl Acad. Sci. USA*, **106**, 20984–20988.

Furukawa, T., Curtis, M.J., Tominey, C.M., Duong, Y.H., Wilcox, B.W., Aggoune, D., Hays, J.B. and Britt, A.B. (2010) A shared DNA-damage-response pathway for induction of stem-cell death by UVB and by gamma irradiation. *DNA Repair (Amst)*, **9**, 940–948.

Genoud, T., Santa Cruz, M.T., Kulisic, T., Sparla, F., Fankhauser, C. and Metraux, J.P. (2008) The protein phosphatase 7 regulates phytochrome signaling in Arabidopsis. *PLoS ONE One*, **3**, e2699.

Gietz, R.D., Triggs-Raine, B., Robbins, A., Graham, K.C. and Woods, R.A. (1997) Identification of proteins that interact with a protein of interest: applications of the yeast two-hybrid system. *Mol. Cell Biochem.* **172**, 67–79.

Grefen, C. and Blatt, M.R. (2012) A 2in1 cloning system enables ratiometric bimolecular fluorescence complementation (rBiFC). *Biotechniques*, **53**, 311–314.

Heidstra, R. and Sabatini, S. (2014) Plant and animal stem cells: similar yet different. *Nat. Rev. Mol. Cell Biol.* **15**, 301–312.

Hellemans, J., Mortier, G., De Paepe, A., Speleman, F. and Vandesompele, J. (2007) qBase relative quantification framework and software for management and automated analysis of real-time quantitative PCR data. *Genome Biol.* **8**, R19.

Heyman, J., Cools, T., Vandenbussche, F. *et al.* (2013) ERF115 controls root quiescent center cell division and stem cell replenishment. *Science*, **342**, 860–863.

Horvath, B.M., Kourova, H., Nagy, S. *et al.* (2017) Arabidopsis RETINOBLASTOMA RELATED directly regulates DNA damage responses through functions beyond cell cycle control. *EMBO J.* **36**, 1261–1278.

Hu, Z., Cools, T. and De Veylder, L. (2016) Mechanisms used by plants to cope with DNA damage. *Annu. Rev. Plant Biol.* **67**, 439–462.

Ikeda, Y., Pelissier, T., Bourguet, P., Becker, C., Pouch-Pelissier, M.N., Pogorelcnik, R., Weingartner, M., Weigel, D., Deragon, J.M. and Mathieu, O. (2017) Arabidopsis proteins with a transposon-related domain act in gene silencing. *Nat. Commun.* **8**, 15122.

Jia, N., Liu, X. and Gao, H. (2016) A DNA2 homolog is required for DNA damage repair, cell cycle regulation, and meristem maintenance in plants. *Plant Physiol.* **171**, 318–333.

Johnson, R.A., Conklin, P.A., Tjahjadi, M., Missirian, V., Toal, T., Brady, S.M. and Britt, A.B. (2018) SUPPRESSOR OF GAMMA RESPONSE1 links DNA damage response to organ regeneration. *Plant Physiol.* **176**, 1665–1675.

Kosugi, S., Hasebe, M., Tomita, M. and Yanagawa, H. (2009) Systematic identification of cell cycle-dependent yeast nucleocytoplasmic shuttling proteins by prediction of composite motifs. *Proc. Natl Acad. Sci. USA*, **106**, 10171–10176.

Kurihara, Y., Matsui, A., Kawashima, M. *et al.* (2008) Identification of the candidate genes regulated by RNA-directed DNA methylation in Arabidopsis. *Biochem. Biophys. Res. Commun.* **376**, 553–557.

Liao, Y., Smyth, G.K. and Shi, W. (2014) featureCounts: an efficient general purpose program for assigning sequence reads to genomic features. *Bioinformatics*, **30**, 923–930.

Love, M.I., Huber, W. and Anders, S. (2014) Moderated estimation of fold change and dispersion for RNA-seq data with DESeq2. *Genome Biol.* **15**, 550.

Ma, J., Liu, Y., Zhou, W., Zhu, Y., Dong, A. and Shen, W.H. (2018) Histone chaperones play crucial roles in maintenance of stem cell niche during plant root development. *Plant J.* **95**, 86–100.

Moissiard, G., Cokus, S.J., Cary, J. *et al.* (2012) MORC family ATPases required for heterochromatin condensation and gene silencing. *Science*, **336**, 1448–1451.

Moller, S.G., Kim, Y.S., Kunkel, T. and Chua, N.H. (2003) PP7 is a positive regulator of blue light signaling in Arabidopsis. *Plant Cell*, **15**, 1111–1119.

Nisa, M.U., Huang, Y., Benhamed, M. and Raynaud, C. (2019) The plant DNA damage response: signaling pathways leading to growth inhibition and putative role in response to stress conditions. *Front. Plant Sci.* **10**, 653.

Raya-Gonzalez, J., Oropeza-Aburto, A., Lopez-Bucio, J.S., Guevara-Garcia, A.A., de Veylder, L., Lopez-Bucio, J. and Herrera-Estrella, L. (2018) MEDIATOR18 influences Arabidopsis root architecture, represses auxin signaling and is a critical factor for cell viability in root meristems. *Plant J.* **96**, 895–909.

Reiterer, V., Eyers, P.A. and Farhan, H. (2014) Day of the dead: pseudokinases and pseudophosphatases in physiology and disease. *Trends Cell Biol.* **24**, 489–505.

Sancar, A., Lindsey-Boltz, L.A., Unsal-Kacmaz, K. and Linn, S. (2004) Molecular mechanisms of mammalian DNA repair and the DNA damage checkpoints. *Annu. Rev. Biochem.* **73**, 39–85.

Sjogren, C.A., Bolaris, S.C. and Larsen, P.B. (2015) Aluminum-dependent terminal differentiation of the Arabidopsis root tip is mediated through an ATR-, ALT2-, and SOG1-regulated transcriptional response. *Plant Cell*, **27**, 2501–2515.

Sun, X., Kang, X. and Ni, M. (2012) Hypersensitive to red and blue 1 and its modification by protein phosphatase 7 are implicated in the control of Arabidopsis stomatal aperture. *PLoS Genet.* **8**, e1002674.

Truernit, E., Bauby, H., Dubreucq, B., Grandjean, O., Runions, J., Barthelemy, J. and Palauqui, J.C. (2008) High-resolution whole-mount imaging of three-dimensional tissue organization and gene expression enables

the study of Phloem development and structure in Arabidopsis. *Plant Cell*, **20**, 1494–1503.

Tsukahara, S., Kobayashi, A., Kawabe, A., Mathieu, O., Miura, A. and Kakutani, T. (2009) Bursts of retrotransposition reproduced in Arabidopsis. *Nature*, **461**, 423–426.

Uhlken, C., Horvath, B., Stadler, R., Sauer, N. and Weingartner, M. (2014a) MAIN-LIKE1 is a crucial factor for correct cell division and differentiation in *Arabidopsis thaliana*. *Plant J.* **78**, 107–120.

Uhlken, C., Hoth, S. and Weingartner, M. (2014b) MAIL1 is essential for development of the primary root but not of anchor roots. *Plant Signal Behav.* **9**, e976477.

Uhrig, R.G., Labandera, A.M. and Moorhead, G.B. (2013) Arabidopsis PPP family of serine/threonine protein phosphatases: many targets but few engines. *Trends Plant Sci.* **18**, 505–513.

Wang, J., Blevins, T., Podicheti, R., Haag, J.R., Tan, E.H., Wang, F. and Pikaard, C.S. (2017) Mutation of Arabidopsis SMC4 identifies condensin as a corepressor of pericentromeric transposons and conditionally expressed genes. *Genes Dev.* **31**, 1601–1614.

Wendrich, J.R., Boeren, S., Moller, B.K., Weijers, D. and De Rybel, B. (2017a) In vivo identification of plant protein complexes using IP-MS/MS. *Methods Mol. Biol.* **1497**, 147–158.

Wendrich, J.R., Moller, B.K., Li, S., Saiga, S., Sozzani, R., Benfey, P.N., De Rybel, B. and Weijers, D. (2017b) Framework for gradual progression of cell ontogeny in the Arabidopsis root meristem. *Proc. Natl Acad. Sci. USA*, **114**, E8922–E8929.

Wenig, U., Meyer, S., Stadler, R., Fischer, S., Werner, D., Lauter, A., Melzer, M., Hoth, S., Weingartner, M. and Sauer, N. (2013) Identification of MAIN, a factor involved in genome stability in the meristems of *Arabidopsis thaliana*. *Plant J.* **75**, 469–483.

Xu, D., Marino, G., Klingl, A., Enderle, B., Monte, E., Kurth, J., Hiltbrunner, A., Leister, D. and Kleine, T. (2019) Extrachloroplastic PP7L functions in chloroplast development and abiotic stress tolerance. *Plant Physiol.* **180**, 323–341.

Yi, D., Alvim Kamei, C.L., Cools, T. *et al.* (2014) The arabidopsis SIAMESE-RELATED cyclin-dependent kinase inhibitors SMR5 and SMR7 regulate the DNA damage checkpoint in response to reactive oxygen species. *Plant Cell*, **26**, 296–309.

Yoshiyama, K., Conklin, P.A., Huefner, N.D. and Britt, A.B. (2009) Suppressor of gamma response 1 (SOG1) encodes a putative transcription factor governing multiple responses to DNA damage. *Proc. Natl Acad. Sci. USA*, **106**, 12843–12848.

Yoshiyama, K.O., Kobayashi, J., Ogita, N., Ueda, M., Kimura, S., Maki, H. and Umeda, M. (2013) ATM-mediated phosphorylation of SOG1 is essential for the DNA damage response in Arabidopsis. *EMBO Rep.* **14**, 817–822.

Yoshiyama, K.O., Kaminoyama, K., Sakamoto, T. and Kimura, S. (2017) Increased phosphorylation of Ser-Gln sites on SUPPRESSOR OF GAMMA RESPONSE1 strengthens the DNA damage response in *Arabidopsis thaliana*. *Plant Cell*, **29**, 3255–3268.